Proceedings of the Twentieth (2010) International Offshore and Polar Engineering Conference
Beijing, China, June 20–25, 2010

ISBN 978-1-880653-77-7 (Set); ISSN 1098-6189 (Set); www.isope.org

Thin Ice Thickness Measured by Upward-Looking Sonar in a Marginal Sea

Jie Su[1], Bo Yang[1], Shunying Ji[2] and Ling Du[1]
1. Key Laboratory of Physical Oceanography of State Education Ministry, Ocean University of China, Qingdao, China
2. State Key Laboratory of Structural Analysis for Industrial Equipment, Dalian University of Technology, Dalian, China

ABSTRACT

Upward-looking sonar (ULS) has been used successfully to observe ice thickness in polar regions since the 1990s, but studies of applying ULS to the measurement of thin ice are rare. In the 2003/2004 winter, a ULS was deployed to measure ice thickness at an oil platform in Bohai Sea. The data, with a relatively high sampling frequency, were transmitted through a cable from the observation system and stored in a computer set on the platform and also sent to a remote computer in real time. A practical model to derive the thickness of thin ice in the marginal ice zones is developed. In the Bohai Sea, the tide is one of the significant hydrodynamic features. The role of tide in affecting the residual total error in the determined mean ice thickness is discussed. The results of sea ice thicknesses derived with the model were compared to observations and estimates from analysis of digital camera images. The model shows reasonable skill in detecting ice less than 0.5 m thick.

KEY WORDS: ULS; marginal sea; sea ice thickness, tide

1. INTRODUCTION

The sea ice cover and its variations in thickness in middle-high-latitude marginal seas are important factors affecting local shipping management, coastal engineering and the safety of oil platforms. Thin ice with a very short life cycle in marginal seas, such as in the Bohai Sea of China, is different from that in the polar regions. It occurs only in winter in the Bohai Sea. The ice conditions of the one-year old ice also show interannual variability, which is related to ENSO cycles (Bai et al. 2001). The Bohai Sea was almost entirely covered by ice in 1969; however the conditions have been mild in most of the years since 1986. With the tendency for global warming, the ice condition in Bohai Sea may provide an index of climate change. Ice measurements, such as ice thickness, ice concentration and ice area, are also important for the initial fields of the numerical sea ice forecast, for forecast verification, and for predicting extreme ice hazards.

Sea ice thickness is an element which is difficult and expensive to measure either directly or remotely. Thickness data observed directly from holes drilled through the ice are highly accurate, but generally have poor spatial and temporal coverage. Direct on-ice observations of thin ice conditions in marginal zones could be very dangerous and are highly dependent on weather and sea conditions. To measure sea ice thickness remotely, inductive radar is an option for multiyear ice floes, but still has challenges for unconsolidated first-year ice (Melling et al., 1995). Upward-looking sonars (ULSs) mounted on submarines have been measuring sea ice draft and ridging characteristics in the basins of the Arctic Ocean for several decades. Great efforts have been made recently in developing moored self-contained ULSs for detecting sea ice at fixed locations in the polar regions (Strass, 1998). Many ULSs have provided high quality sea ice draft estimates since the mid-1990s. A moored ULS has been developed to measure the underside topography of the polar pack ice (Melling et al., 1995). Fukamachi et al. (2003) examined the variability of sea-ice draft off Hokkaido in the Sea of Okhotsk based on the observations of a ULS along with an ADCP. Based on the observations of three ULS systems, deployed in the north-western Barents Sea for 2 years, it is suggested that the transport of ice from the Central Arctic into the Barents Sea appears to be associated with the large-scale variations such as the AO/NAO (Abrahamsen et al., 2006). The ULS was also used in examining the behavior of the Bering Sea St. Lawrence Island polynya, along with satellite imagery and salinity/temperature measurements (Drucker et al., 2003). However, difficulties remain applying this technology for thin ice in marginal ice zones. This is mainly due to the fact that the sonar echo signal reflected from thin ice less than 0.7 m is very weak, so that the calculated ice thickness is not reliable. The relatively strong tidal currents in the marginal sea also affect the accuracy of this technology. For one-year old thin ice, few ULSs have been used successfully.

This paper is organized as follows: Section 2 describes the setup of a ULS system installed in Bohai Sea and the data recorded by the instrument; section 3 provides the data processing method, with an emphasis on the effect of the tides; it also compares the processed sea ice thickness data with the observations; the last section is the conclusion.

2. INSTRUMENTS AND DATA

A typical ULS system usually includes a sonar and a high precision

pressure sensor, with the former emitting the pulses of sound towards the bottom of floating ice and measuring the travel time t triggered by the return pulse, and the latter measuring the static pressure of water P_b. Based on profiles of temperature and salinity, the effective velocity of sound v and the mean water density ρ from instrument to ice bottom can be estimated. The distance between the sonar and the ice bottom is calculated from

$$r=v\,t/2 \quad (1)$$

The depth h of pressure sensor below sea level is estimated from

$$h=(P_b-P_a)/\rho\,g \quad (2)$$

where P_a is the atmosphere pressure at the surface, g is the acceleration of gravity. Then the ice draft d is determined by

$$d=h-r \quad (3)$$

Thus the ice thickness of the whole ice floe can be calculated through the buoyancy formula:

$$D=d\,\rho_{wo}/\rho_i \quad (4)$$

where ρ_{wo} and ρ_i are the surface water density and ice density.

In the winter of 2003/2004, a seabed-mounted ice measuring system, manufactured by the National Ocean Technology Center of State Oceanic Administration (SOA) of China, was installed on the JZ120-2 Platform of Bohai Sea of China (Fig.1). The water depth in this location is 18m. The ULS system consists of a sonar, a static pressure sensor, and a temperature and salinity sensor. To measure highly accurate transit times, a signal of linear frequency modulation (chirp signal) emitted by the sonar was used (Guo et al., 2005). An underwater cable connecting the system and platform was used to provide power for the equipment and to transmit data from the equipment to a controlling computer on the platform. Other vital data, such as barometric pressure, were also input to the computer by a Local Area Network (LAN). Raw data were processed and the preliminary results were displayed in real time by the computer mounted on the platform. The preliminary results were emailed to the remote computer user on the shore.

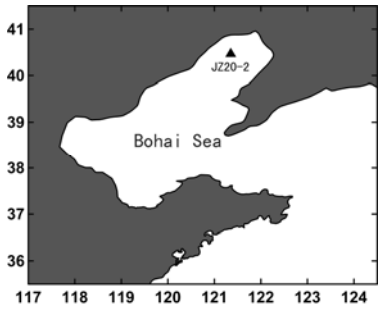

Fig. 1 Map of the Bohai Sea. The solid triangle shows the location of the ULS system.

Without limitations of memory storage and battery power, the sampling interval could be specified relatively freely. We sampled atmospheric pressure, static pressure and travel time of the echo every 10 min. During each sampling cycle, first, 60 pressure measurements were obtained at 1 second intervals, followed by 20 observations of T/S at the bottom. Then, the sonar sent a burst of 120 sound pulses offset by 1 second.

3. METHOD AND RESULTS

The ice thickness model includes several steps to reduce the error. The main steps include revision of the sound velocity profile, ice-water discrimination, rejection of obviously erroneous data, and adjustment of the surface level.

3.1 Sound velocity profile

To estimate accurately the distance between instrument and the ice bottom based on the sound travel time and the water depth derived from the static pressure, profiles of sound speed and water density are needed. To do this, we must know the vertical distributions of T/S through the water column during the measurement. However, there were many sources of noise in the surface layer near the platform that could affect sensor performance; moreover, since it is difficult to mount a temperature and salinity sensor in the surface layer and avoid the noise of the platform at the same time, we mounted the T/S sensors on the bottom together with the sonar equipment. During most of the winter, the sea water in Bohai Sea is mixed relatively well, especially at shallow depths. The water depth of the Platform JZ20-2 is only about 18m. Thus temperature and salinity were taken as constant for the whole water column for the calculation of ice draft. However, the error caused by this assumption must be estimated. Fig. 2 displays profiles of T/S from a CTD cast when the equipment was recovered on Feb. 20, 2004. Although the profiles are noisy, which is mainly due to the motion of the CTD during its deployment, vertical variations of temperature and salinity are evident. The surface temperature is slightly higher than the bottom value, with a difference of 0.1 °C; the salinity is almost vertically uniform with a difference between the surface and bottom of about 0.02-0.04. The vertically averaged temperature and salinity are -1.08 °C and 34.22. We have noticed that, at the time the profile was taken, the weather was warming up and the sea ice was disappearing. So this profile could not represent the T/S profile during ice covered season when the surface temperature was slightly lower than the bottom value. Error analysis indicates that the observing system is more sensitive to temperature than salinity. If the pattern of T/S profiles does not change substantially, the distance errors associated with sound velocity and density displacement are estimated as ~10^{-3}m, using depth-invariant T/S distributions with values measured at the bottom instead of complete profiles.

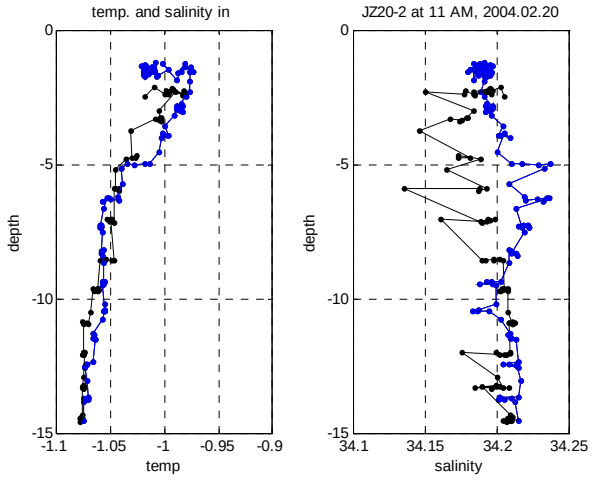

Fig. 2 Vertical structures of the temperature and salinity measured with a CTD when the ULS was recovered on Feb. 20, 2004. (blue line: CTD downward profile; black line: CTD upward profile)

3.2 Ice-water discrimination

Before the calculation of ice draft, it must first be established whether ice or water is present, i.e. ice-water discrimination. For ice-free water, the draft value calculated from sonar echoes and static pressure is zero in theory. But in fact, it is impossible to find the open water periods by simply taking a draft measurement $d = 0$ as the indicator. This is because: (1) the sound velocity model is not fully capable to distinguish between thin ice and open water, and (2) the downward displacement of an open water surface by wind waves may lead to faulty classification

as ice covered (Strass, 1998). Thus, we rarely use Eq. 3 to estimate the draft directly. In Bohai Sea, it is even difficult to tell whether it is ice or open water only by the draft value, since the value of draft in open water conditions may have the same magnitude as the typical ice thickness. With high wind and waves, the draft value can fluctuate and have values greater than the typical ice thickness. Therefore, ice-water discrimination is an important step during data processing and auxiliary variables are needed.

Strass (1998) used two important auxiliary variables, V_{en} and $D_{dif.}$ V_{en} is envelope voltage which is associated with the echo amplitude and also could be assumed as a measure of the target strength of the interface from which the echo returns. D_{dif} is defined as the difference of the two most similar draft measurements, in each 4-pulse burst. Choosing V_{en} as one of the auxiliary variables is based on the fact that the value of V_{en} at air-water interface is generally higher than that at ice-water interface. This is because that the sound signal reflectivity is higher at an air-water interface than that at an ice-water interface. However, V_{en} values at two different interfaces can only be distinguished under calm conditions. During periods of high winds and waves, V_{en} is not an effective measure of ice presence or absence. With surface waves, the increasing sea surface roughness causes larger scattering of sound energy, resulting in lower amplitude of the echo. Surface roughness can be deduced from the short-term draft variations of adjacent sonar pulses by D_{dif}.

Our work has some features that are different from Strass's research and some other previous studies on ice thickness measured by sonar. First, our work mainly focuses on thin ice, while theirs dealt with thick ice. Second, in most previous work, the ULS data are stored in self-contained memory and processed off-line after the instrument is recovered. For each burst, the number of samples is limited. With the mass storage in the computer at the platform, we can acquire more samples (as many as 120 sonar pulse) in each burst. This allows us to extract more information by using statistical methods. In our earlier paper (Guo et al., 2005), two auxiliary variables and their critical values were mentioned. In this part, we will give the details about how the variables are defined and the critical values are determined.

Based on experiments in labs and at the platform, we discovered that V_{enm} (the mean V_{en}) and D_{sigm} (the variance of d) in a burst are better auxiliary variables of water/ice discrimination for thin ice with a higher frequency of data records. Moreover, they can represent more integral statistical information then V_{en} and D_{dif}. Under calm conditions, V_{enm} usually is small when sound pulses return from the ice bottom, and is large when those return from the ice-free sea surface. However, with high wind speed and waves, sound energy is scattered intensively. Therefore, whether the sea surface is covered by ice or not, V_{enm} would be very small. Fortunately, wind plays a minor role in affecting the variation of ice draft. Apparent draft varies significantly under an ice-free surface compared to that under an ice-covered surface. This means that V_{enm} and D_{sigm} together could be criteria to discriminate between ice-covered or ice free conditions.

We designate the data in each 10 minute sampling period as a group. For each group of data, a processing scheme based on a running filter with a window length of 11 was designed. Thus, for each burst of 120 raw data points, 110 values of V_{enm} and D_{sigm} can be calculated. Two typical time periods, from Jan. 4 to 12 (open water, Fig. 3) and from Jan. 16 to 26 (ice-covered surface, Fig. 4), were selected for statistical analysis the distributions of the parameters. Fig. 3 and 4 are histograms of the frequency of occurrence of the strength of the signal of the indicated variables. The value of V_{en} and V_{enm} are directly proportional to the echo amplitude. Both have strong, well-defined peaks between 10 and 20 (Fig. 3), while peak values during ice-covered period found less than 10 (Fig. 4). For D_{sigm}, the peak is less than 0.001 during ice-covered period and much larger during ice-free period. It should be noted that the units of horizontal axes of the bottom panels in Fig. 3 and Fig. 4 are different. Additional statistical analysis under different wind speed indicates that 12 for V_{enm} and 0.001 for D_{sigm} are acceptable critical values for the ice-water discrimination. When these two variables are both less than the critical value, the data point is judged as ice. This combined criterion is a strict one, which means that for open water, a data point would not be categorized as one with ice present. However, by applying this criterion for mixed surface conditions, i.e., where ice floes pass the ULS view window with gaps of water, some data points obtained under ice may be marked as open water. These criteria using V_{enm} and D_{sigm} for water/ice discrimination are suitable for ice detection during our study, especially the first day and the last day ice appeared (Guo et al., 2005).

Therefore, in one sampling group, 110 effective values of the draft d were obtained, with some marked as open water points and others marked as ice points. In some situations, all d may be marked as open water points or ice points in a group. All drafts marked as ice point are averaged to represent the average ice draft for that burst (group).

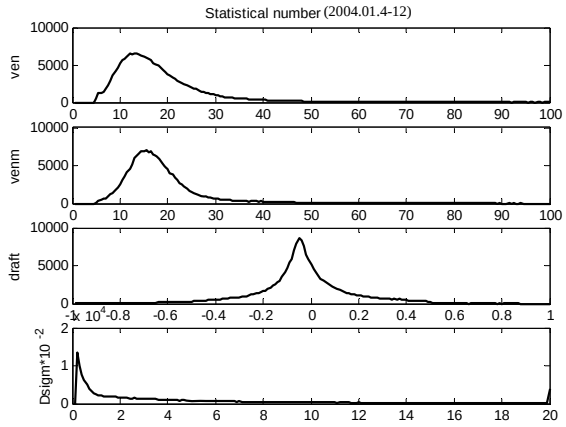

Fig. 3 Statistics of V_{en}, V_{enm}, draft and D_{sigm} during a period of open water condition (2004.01.04-12)
(The x-axis indicates the value of the parameters V_{en}, V_{enm}, draft and D_{sigm}, the y-axis indicates the frequency of occurrence of the value of the designated variable over the observation period.)

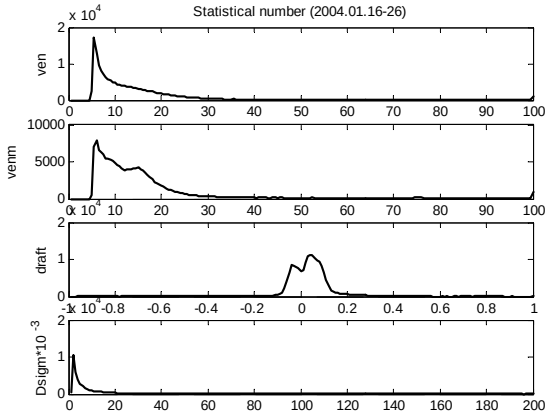

Fig. 4 Statistics of V_{en}, V_{enm}, draft and D_{sigm} during a period of ice-covered condition (2004.01.16-26) See Fig. 3.

3.3 Adjustment of the surface level

The final ice draft is obtained from the above average ice draft minus the sea surface level. We can also get the average water draft of one burst by averaging all drafts marked as water point in a sampling group. As we mentioned above, the averaged open water draft is not always equal to 0, which means a correction for the surface level needs to be applied. This step of the data procedure is called adjustment of the surface level.

The blue line in Fig. 5 shows the average water draft (a) and average ice draft (b) of each burst during the operation time. If we assume that all of the water points were correctly assigned, the average water draft can provide a measure of the fluctuating sea surface level. Since in theory the value of those water drafts are zero, we call it sea level offset. Strass (1998) indicated sea level offset was mainly due to the deficiencies of the empirical sound velocity model. He used an automated procedure to calculate the sea level offset during ice-free period by averaging the drafts in a week long time period, and used an interactive graphics program to determine sea level offset during an ice-covered period.

In our work, the water point draft (Fig. 5a, blue line) shows many large values, especially in the ice-covered period. Most large values are caused by errors of water/ice discrimination since the criteria are well defined for ice points. Some of them are due to strong winds and big waves. But from Fig. 5a, we can see that the values of the draft are much smaller during ice free period (before Jan. 13 and after Feb. 9). The water point draft in Fig. 5a also indicates a strong semi-diurnal variability, with typical amplitude of ~2×10^{-2}m, especially in the ice free period. Thus, simply averaging the draft labeled as water either during ice-covered period or during ice-free period is not a good way to get the sea level offset. A method that can remove the tidal signal should be used.

First, we used T_tide (Pawlowicz et al. 2002) to analyze the water point draft during the ice free period. The result shows a strong M_2 tide-like signal in the time series (Fig. 5, red line). This fluctuation should be related to the semi-diurnal tidal currents in the Bohai Sea. This phenomenon has not been reported by any other ULS users who collect observations from the deep oceans, where tidal currents are relatively weak. Then we used the time series as the sea level offset and obtained the final ice point drafts throughout the observation period.

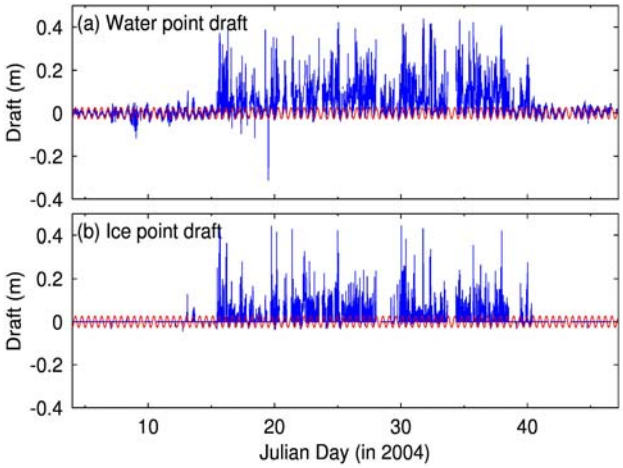

Fig. 5 Water point draft (a, blue) and ice point draft (b, blue) before adjustment of sea level, and M_2 tide-like signal predicted by T_tide (red)

To investigate the mechanism of the fluctuation of the sea level offset further, we zoom in the first 3 days of Fig. 5a and examine the relationship with observed bottom temperature and model calculated tidal currents [Yang, personal communication]. At the location of the platform, the tidal flow field is dominated by semi-diurnal reversing currents with northeast/southwest directions. Fig. 6c shows the currents along the major axis, with a positive value indicating a northeastward inflow.

Compared to the tidal currents, the open water draft has a phase-shift of π radians, which means the open water draft reaches its minimum when the northeastward inflow is at its peak. For the empirical model adopted in our method, the sound velocity is mainly determined by the temperature. The temperature also has a semi-diurnal variation (Fig. 6b) with a phase lag of about $\pi/2$ relative to the tidal currents. The observed temperature increases during the flood tide (when the tidal currents in Fig. 6c are positive), while it decreases during the ebb tide. This agrees with the general knowledge of the horizontal distribution of the temperature in winter: water in the central Bohai Sea is relatively warm, whereas, water at the head of the bay is relatively cold.

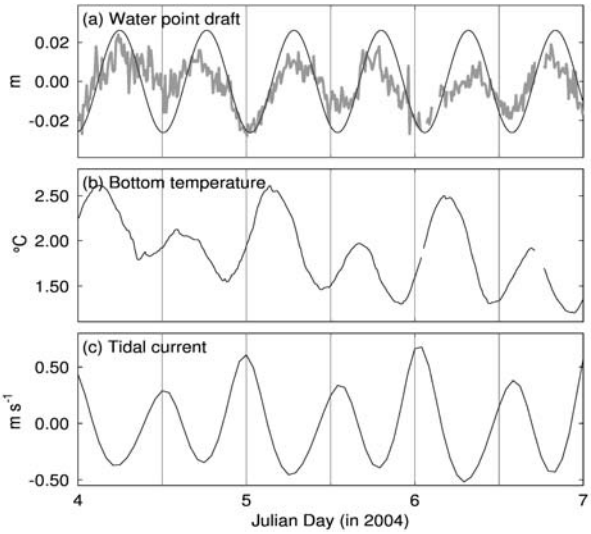

Fig. 6 (a) Water point draft (gray) and M_2 tide-like signal predicted by T_tide (black) from Fig. 5a, (b) observed bottom temperature, (c) model calculated tidal current, with positive values indicating northeastward inflows.

During the observation period, no profiles of T/S were obtained, so the exact temporal variation of the T/S vertical structure is unknown. From the analysis of several profiles observed at other stations in Bohai Sea in different winters during the ice season, it is quite certain that the surface temperature is lower than the bottom one. On the other hand, during seasons without ice, the surface temperature is usually higher than that at the bottom. In our calculation, the water properties were assumed vertically uniform. If the pattern of the temperature structure does not change with the tides, the systematic error can be minimized by imbedding an artificial profile in the empirical models as Strass (1998) did. However, if the temperature structure changes with tidal phase, the depth-mean temperature could be overestimated during one tidal phase, and underestimated at another, based on the measurements at the bottom. This could partially explain the M_2 tide-like variability of the sea level offset. Error analysis indicates that for a water column with the depth of ~ 20 m, an error of 1°C in depth-mean temperature results in the error of 0.4×10^{-2} m in h based on the static pressure and the error of 7.5×10^{-2} m in r based on sonar pulses.

Therefore, only the error associated with sonar pulses are discussed here. When the depth-mean temperature is overestimated, the calculated sound velocity is also overestimated, resulting in an r that is too high. Thus, the draft d is underestimated (Eq. 3). In our case, the water point draft d is underestimated (overestimated) during the flood (ebb) tide, which suggests that the near-surface temperature is overestimated (underestimated) when the water inflows (outflows).

The vertical structure of temperature during the operation time is unknown. Fortunately, two 24-hour time series of near-surface and near-bottom temperatures in platform JZ20-2 were obtained on Jan. 8, 2010 (Fig. 7a). Although the surface temperature must be calibrated after the sensor recovered in the future, the semi-diurnal variations in the two series are evident. The near-bottom temperature (Fig. 7a, gray line) has its maximums at 7.5 and 21.5 hours, except for the spikes (The exact reason of the occurrence of spikes is unknown), with a phase lag of 0.5~1.5 hours relative to tidal currents, in the same direction as in Fig. 6 but substantially smaller. The variation of the near-surface temperature is opposite to that of the bottom series. The differences between the surface and bottom temperatures change with the tide in a range of 0.6~1.0 °C.

While it is evident that there are problems with the surface record, we do believe that the temperature of the two records represent the true relative variation at the site. During the flood tide, the near-bottom temperature increases, while the near-surface temperature decreases. This may be mainly due to a stronger stratification in the deep water. In the sound model, the near-surface temperature is overestimated based on the bottom observations, compared to a time-invariant profile. While during the ebb tide, the near-surface temperature is underestimated.

This fluctuation in the structure of the temperature profile results in a fluctuation in the sea level offset with the order of 10^{-2} m. Therefore, the mechanism of the semi-diurnal tide-like signal in the sea level offset can be partially explained. Then the ice draft (Fig. 5b, blue line) is corrected by subtracting the sea level offset (Fig. 5b, red line).

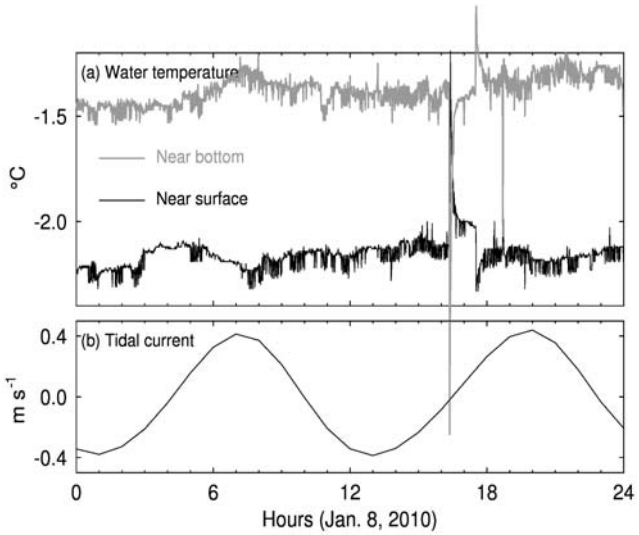

Fig. 7 (a) Observed near-surface (black) and near-bottom (gray) temperature and (b) model calculated tidal currents on Jan. 8, 2000. The positive values indicate the northeastward inflows.

To convert the corrected ice draft to ice thickness, a constant value of 836 kg m^{-3} for the ice density ρ_i in Eq. 4 was used based on the ice density measurements provided by National Marine Environmental Forecasting Center of China. Water density also changes with the tide, since temperature changes. But as discussed above, this change is minor compared to the changes due to variation of the sound speed profile. Therefore, the surface water density ρ_{wo} is estimated as 1024.5 kg m^{-3} in the calculation of buoyancy formula.

During the data processing, parameters including temperature, salinity, static pressure were also examined for erroneous data.

3.4 Result Comparison

The ice thickness estimates obtained from the processed ULS system is compared with two other kinds of observations. One is visual ice thickness based on the observations of ice type around the JZ20-2 Platform. This method gives a range of ice thickness instead of a unique value. Another estimate is from the analysis of images obtained by a digital camera installed on the platform. When ice encounters the platform, it is broken and piled up. A lens cap, used as a reference, is also captured in the digital images with the broken and piled up ice floes. Then the ice thickness was estimated relative to the known diameter of the lens cap.

Both these methods provide data during daylight hours. Fig. 8 shows the comparison of the model results and these two types of observations. Fig. 9 focuses on data from six individual dates. It should be noted that only the thickness of the flat ice (level ice) is estimated by both observations, while the ULS may capture the ice tilt associated with broken and overlapping floes. We expect then that the ULS-based data will generally have larger thicknesses than those estimated by the other methods. Thus most of the large thickness values estimated by the ULS in Fig. 8 could be reasonable. In general, our model reproduces reasonably well the observed ice thickness. It also captures the time when the ice occurs and disappears in that winter. The probability density distribution for the level ice shows that the ice thickness at this location can exceed 20 cm (Ji et al., 2002). But during 2003/2004 winter, the observed level ice thickness is no more than 20cm. Except for the calculation error, all the values larger than 20cm should be due to ice tilted and piled up.

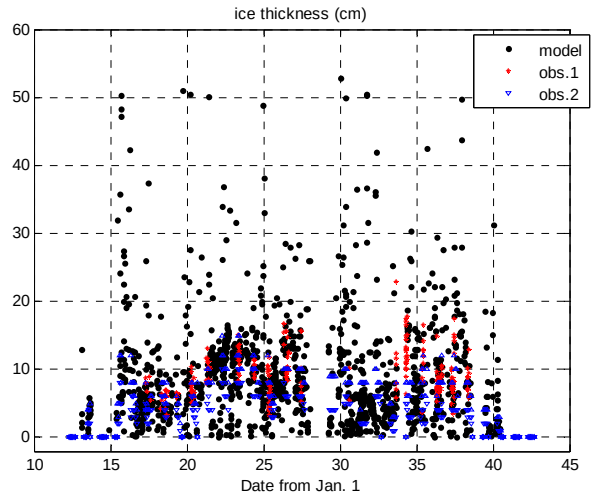

Fig. 8 Comparison of ice thickness estimated by ULS (black dot) and optical observations based on visual (blue triangle) and on digital camera images (red star).

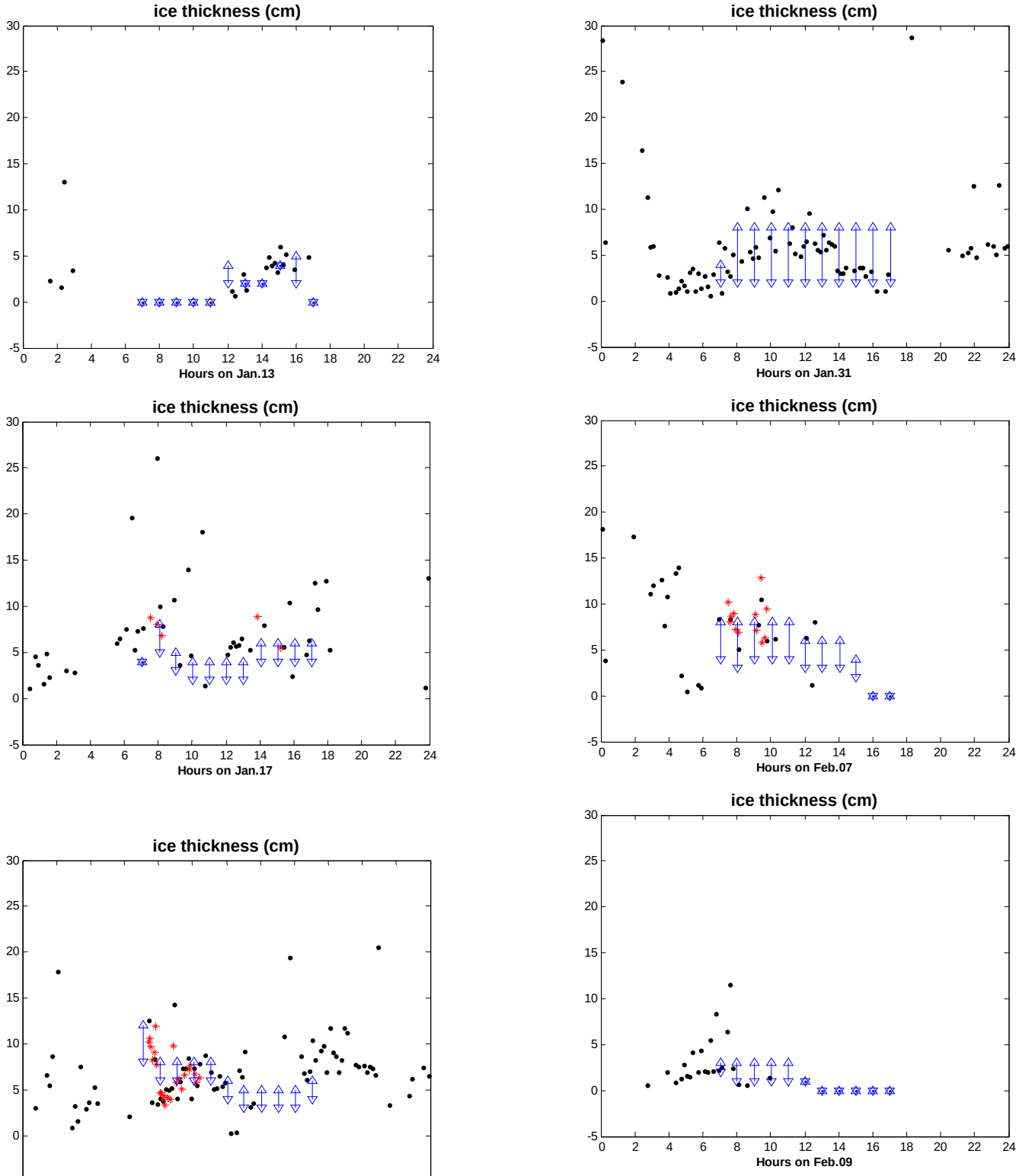

Fig. 9 Comparison of modeled ice thickness and observations in several days (description of the figures is the same as figure 8)

4. CONCLUSIONS

An upward-looking sonar (ULS) was deployed at a platform in Bohai Sea to measure ice thickness in the 2003/2004 winter. A practical, robust ice thickness model to derive the thickness of thin (<50cm) ice

in the marginal ice zone was developed based on the strength of the return signal and variance of ice draft from acoustic burst sampling. The critical values of two auxiliary parameters for ice-water discrimination were determined based on the experimental data and shown to be valid throughout the winter.

In the Bohai Sea, the tide is one of the significant hydrodynamic features. The M_2 signal in the sea level offset is mainly associated with the tide-dependent vertical structure of temperature. The amplitude of the tide-induced sea level offset is ~2 cm. Unlike the method developed for the ULSs in previous studies, the adjustment of the surface is applied by subtracting this M_2 tide-like signal.

To assess the performance of the method, images obtained by a digital camera installed at the platform and visual observations were processed. Compared with the observations, this derived model has reasonable skills in detecting ice less than 0.5 m thick.

ACKNOWLEDGEMENTS

This study was supported by the National High Technology Research and Development Program of China (863 project) under contract No. 2008AA121701 and the National Natural Science Foundation of China under contract No. 40876003 and 40631006. The data is comes from a previous 863 project (No. 2001AA631070W). Thank for Senior Engineer Jijie Guo's cooperation in manufacturing the sonar equipment and providing the raw sonar data. Thanks Professor Jinpin Zhao for his endeavor and support to 863 projects. We also thank Dr. Brian Petrie for reading the manuscript and providing useful comments that improved the paper.

REFERENCES

Abrahamsen, EP, Osterhus, S, and Gammelsrod, T (2006). "Ice Draft and Current Measurements from the North-western Barrents Sea, 1993-96," *Polar research*, Vol 25, No 1, pp 25-37

Bai, S, Liu, Q, and Wu, H (2001). "Relation of Ice Conditions to Climate Change in Bohai Sea of China", *Acta Oceanologica Sinica*, Vol 20, No 3, pp 331-342.

Drucker, R, Martin, S, and Moritz, R (2003), "Observations of Ice Thickness and Frazil Ice in the St. Lawrence Island Polynya from Satellite Imagery, Upward Looking Sonar, and Salinity/temperature Morrings," *Journal of Geophysical Research*, Vol 108, No C5, pp 3149,18-1-18-18

Fukamachi, Y, Mizuta, G, Ohshima, K.I, Melling H, Fissel, D, and Wakatsuchi, M (2003), "Variability of Sea-ice Draft off Hokkaido in the Sea of Okhotsk Revealed by a Moored Ice-profiling Sonar in Winter of 1999," *Geophysical Research Letters*, Vol 30, No 7, 29-1-4.

Guo, J, Su, J, and Yang, B (2005). "Monitoring Sea Ice in Bohai With A Chirp Sonar System," *Proc 18th Int Conf on port and ocean Eng*, Under Arctic Conditions, Vol 2, pp 745-754.

Ji, S, Yue, Q, and Bi, X (2002), "Probability Distribution of Sea Ice Fatigure Parameter in JZ20-2 Sea Area of the Liaodong Bay," *the Ocean Engineering*, Vol 20, No 3, pp 39-43. (in Chinese with abstract in English)

Melling, H, Johnston, PH, and Riedel, DA (1995). "Measurements of the Underside Topography of Sea Ice by Moored Subsea Sonar," *Journal of atmospheric and oceanic technology*, Vol 12, pp 589-602.

Pawlowicz, R, Beardsley, B, and Lentz, S (2002). "Classical tidal harmonic analysis including error estimates in MATLAB using T_TIDE," *Computers and Geosciences*, Vol 28, pp 929–937.

Strass, V.H (1998). "Measuring Sea Ice Draft and Coverage with Moored Upward Looking Sonars," *Deep-sea research I*, Vol 45, pp 795-818.